Fast reaction mechanism of a core(Al)-shell (Al_2O_3) nanoparticle in oxygen

Weiqiang Wang, Richard Clark, Aiichiro Nakano, Rajiv K. Kalia, and Priya Vashishta[a)]
Collaboratory for Advanced Computing and Simulations, Department of Physics and Astronomy, Department of Chemical Engineering and Materials Science, and Department of Computer Science, University of Southern California, Los Angeles, California 90089-0242, USA

(Received 30 July 2009; accepted 3 November 2009; published online 28 December 2009)

Atomistic mechanisms of oxidation in a laser flash heated core (Aluminum)-shell (Alumina) nanoparticle are investigated using multimillion-atom molecular dynamics simulations. We find a thermal-to-mechanochemical transition of oxidation mechanism when the initial core temperature is above 6000 K. The transition from thermal diffusion to mechanically enhanced diffusion to ballistic transport is accompanied by a change in the intermediate reaction products from Al rich Al_2O to oxygen rich AlO_2 clusters. Higher initial temperature of the core causes catastrophic failure of the shell, which provides direct oxidation pathways for core Al, resulting in faster energy release. © *2009 American Institute of Physics*. [doi:10.1063/1.3268436]

Oxidation mechanism of Al nanoparticles (ANP) has drawn a great deal of attention owing to the orders of magnitude increase in the reactivity of the energetic materials containing ANP compared to traditional micron size thermites.[1–5] In these studies, it is found that the diffusion-based oxidization mechanism used to describe the burning of micrometer-size thermites failed to explain the high reactivity of ANP. Alternatively, a melt-dispersion mechanism is proposed based on the spallation of the oxide shell.[3] Experiments using laser flash heating of nano-Al aggregates in polymers showed a linear relationship between the reaction propagation distance and laser energy, which is explained with a hydrodynamic model instead of the thermal explosion model.[6,7] In these models, mechanical breakdown of the ANP's oxide shell is suggested to play an important role,[3,8,9] but the underlying atomistic processes are not yet fully understood due to extremely small space-time scale in the reaction process. Therefore, an understanding of how the ANP starts reacting under different ignition conditions is foreseen as the key to analyzing atomistic mechanism. In this letter, we have used molecular dynamics (MD) to investigate the atomistic mechanisms in oxidation reactions in a laser flash heated core (Al)-shell (Al_2O_3) ANP in an oxygen environment. Ignition of an isothermally heated ANP will be presented later in a separate letter.

All the MD simulations reported here have a single 48 nm ANP with a 4 nm alumina shell embedded in oxygen. A total of 11 018 467 atoms—including 1 928 931 core Al, shell atoms (1 152 528 Al and 1 727 292 O), and 6 210 716 environmental oxygen surrounding the nanoparticle—are contained in a cubic box with edge length of 226.419 nm. Size of the MD box is sufficiently large not to impose boundary effects. A snapshot of the initial configuration is shown in Fig. 1(a).

In the laser flash-heating experiments of ALEX (a commercially available Al nanoparticle aggregates) by Dlott and co-workers,[6,7] the wavelength of laser beam is selected in the near IR regime (~1.06 μm), which is absorbed only by the metal core. In our simulations, the initial conditions are an Al core heated at 3000, 6000, and 9000 K encapsulated in a shell at room temperature. To obtain a uniformly heated core, core atoms are thermalized using MD and Langevin dynamics while keeping the alumina shell atoms fixed. After this preparation, the constraints on the shell atoms are removed and the nanoparticle evolves within microcanonical ensemble.

The modeling of Al_2O_3 is based on an interatomic potential that incorporates ionic and covalent effects through a combination of two- and three-body terms.[10] This potential has been validated by comparing the MD results for structural and mechanical properties of both crystalline and amorphous alumina with the experimental data. For the core Al, we use an embedded atom method potential.[11] To describe the oxidation of Al, we use a bond-order coupling scheme, which has been validated against quantum mechanical results on structural properties of various partially oxidized Al clusters.

To compare the energy release rates in the three systems, the time variation of the average kinetic energy per atom is shown in Fig. 1(b). The observation that higher initial temperature of the Al core releases more energy is not unexpected, and consistent with the experimental results by Dlott and co-workers.[12,13] However, a nonproportional increase in the energy release due to increased core temperature from 3000 to above 6000 K indicates a change in the reaction mechanism.

Reactions in micron size thermites are accompanied by diffusion of atoms. However, the situation in nanothermites

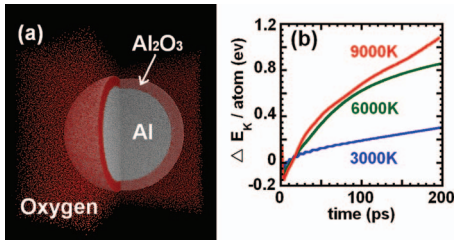

FIG. 1. (Color) (a) Initial setup of the system consisting of a single core-shell nanoparticle embedded in oxygen. Most of the oxygen atoms surrounding the nanoparticle are not shown for clarity. To show the inside, a quarter of the nanoparticle has been removed. (b) Increase of kinetic energy per Al atom in the process of explosion for the C3 (3000 K), C6 (6000 K), and C9 (9000 K) systems.

a)Electronic mail: priyav@usc.edu.

TABLE I. Shell composition (O/Al ratio) in C3, C6, and C9 systems at various times.

	0 ps	30 ps	50 ps	100 ps	150 ps	200 ps
C3	1.5	1.37	1.35	1.32	1.30	1.28
C6	1.5	1.25	1.18	1.11	1.11	1.12
C9	1.5	1.16	1.11	1.08	1.07	1.07

is more complicated depending on the initial heating conditions. Our motivation is to examine the atomistic mechanisms in nanothermites. In our MD simulations, by dividing the system into core, shell, and outside regions, migration of atoms into each region is analyzed in atomistic detail. We identify the shell as the largest covalently bonded aluminum-oxide cluster, and the other two regions are defined on the basis of their relative positions to the shell. We find large number of atoms moving in and out of the shell region in each system. Higher initial core temperature causes more atom-migration events, leading to faster change of the shell stoichiometry. Table I shows the composition of the shell (ratio of O to that of Al atoms) at various times. Higher initial temperature of the core results in faster decrease in the O to Al ratio in the shell as more core Al react with shell oxygen. This in turn leads to faster oxidation of the ANP via easier diffusion of the environmental oxygen through the shell.

Behavior of ANP due to different initial Al core temperatures is shown in Fig. 2, where the first, second, and third rows are snapshots of the C3, C6, and C9 systems, respectively. Initially, each ANP is enclosed by a shell, which protects the Al core from oxidation by environmental oxygen. When the core is heated, the shell responds in a different manner due to different driving forces from the core. The C3 system has the lowest core temperature, resulting in smaller damage to the shell. Oxidation in this case is mainly due to

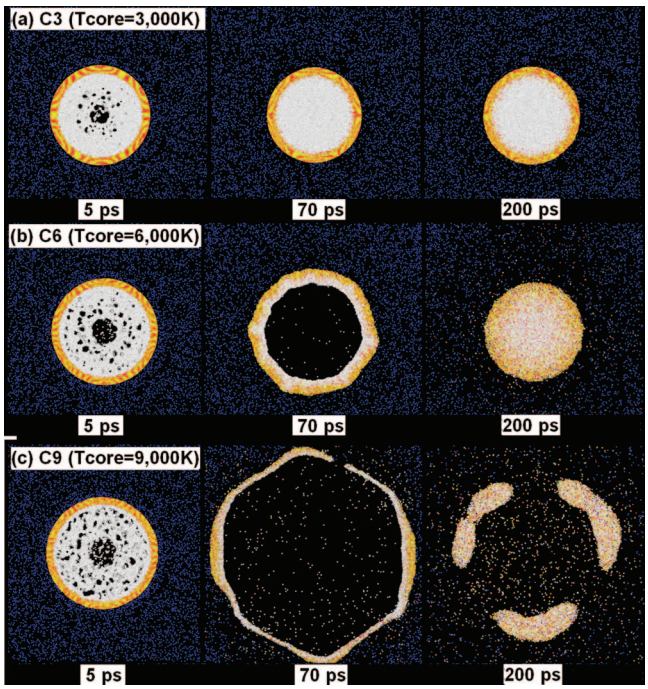

FIG. 2. (Color) Snapshots of the nanoparticle at different times with initial core temperature of (a) 3000, (b) 6000, and (c) 9000 K. The core aluminum is shown as white; shell aluminum, yellow; shell oxygen, red; and environmental oxygen, blue.

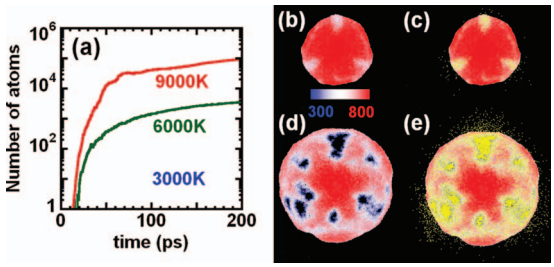

FIG. 3. (Color) (a) Plot of the number of Al core atoms jetting into oxygen in the C3, C6, and C9 systems. (b) and (d) are snapshots of shell morphology in C6 and C9, respectively, at 100 ps with colors representing the number density (in unit of number of atoms/nm^3) in the shell as shown by the color bar. (c) and (e) are snapshots of the shell morphology superimposed with jetting-out core Al atoms (in yellow) for C6 and C9, respectively. Environmental oxygen is not shown for clarity of presentation.

the diffusion of shell oxygen toward the core, where the inward diffusion depth at the core/shell interface is only 3.8 nm at 200 ps. Here, the shell structure is largely unchanged up to 200 ps [see Fig. 2(a)]. Compared to C3, the ANP in C6 first expands to form a hollow cavity inside the nanoparticle at 70 ps and then collapses to fill the cavity and forms a solid body again at 200 ps, but with a considerable penetration of oxygen into the core region. This mechanical expansion/collapse process results in serious damage to the original shell structure and its composition becomes close to $AlO_{1.1}$ (see Table I). Consequently, boundary between the shell and the core is blurred, and some shell oxygen atoms are already seen at the center of the nanoparticle, indicating a remarkable mass transport up to 20 nm within 200 ps. At 200 ps, the environmental oxygen in C6 is 8.9 nm from the center of the ANP, in contrast to 22.5 nm in C3. Oxidation mechanism of the ANP by environmental oxygen after 200 ps will still be via diffusion because of the reconsolidation of the ANP, but with a much faster rate as a result of earlier mechanical mixing by expansion/collapse process—hence mechanically enhanced diffusion. The fastest energy release is seen for the C9 system [see Fig. 1(b)]. Here, detailed analysis of the atom migration events show a mechanism involving ballistic transport of atoms resulting from the opening of pores in the shell [see Fig. 2(c)]. Calculation of shell's minimum thickness shows that pores in the shell appear as early as at 22 ps. This catastrophic mechanical breakdown of the shell removes the protective layer that would prevent further oxidation of the core Al atoms.

Change in reaction mechanisms from defect-induced diffusion processes to nondiffusion processes of mechanochemical effects is proposed for reactions in powder mixtures when changed from shock-assisted reactions to shock-induced reactions.[14] In our MD simulations, we have also found the transition in reaction mechanism from the diffusion between core and shell, assisted by the molten core (melting-core-assisted reaction), to the nondiffusive process due to the catastrophic failure of the shell caused by the high-pressure of the molten core (melting-core-induced-reaction).

Figure 3(a) is a semilog plot of the number of core Al atoms jetting into the environment. The C3 system shows no direct transport of core Al to the outside because of the intact shell. For C6, the number of core Al atoms that cross the shell is in the order of 1000, signifying limited direct oxidation reactions between core Al and environmental oxygen. This number is small because the expansion of the shell

TABLE II. Statistics and chemical composition of the fragments in C3, C6, and C9 systems at 200 ps.

	Al_4O	Al_3O	Al_2O	AlO	Al_2O_3	AlO_2
C3	3235	6508	7998	5332	81	29
C6	1706	6343	15 209	24 894	1658	14 200
C9	126	655	6107	98 828	3185	113 796

driven by the pressure of the core is not large enough to generate distinct pores in the shell. Instead, there are low-density regions in the shell [Fig. 3(b)], through which core Al jet out [Fig. 3(c)]. These low-density regions close up again in the subsequent shrinking phase and prohibit further jetting out of the core Al.

In C9, the number of core Al jetting into oxygen is orders-of-magnitude larger than that in C6 [Fig. 3(a)] due to the opening of large pores in the shell [Fig. 3(d)] that provides pathways for the core Al to directly react with environmental oxygen [Fig. 3(e)]. The large number of ballistically transported core Al into the environment results in the fastest energy release rate for C9, and permanent opening of pores in the shell of C9 ensures continuous oxidation of the core Al even after 100 ps [Fig. 1(b)].

Simulations of the oxidation of Al clusters[15] and experiments[13,16] of the laser ablation of Al films have all shown the production of many intermediate reaction products, which are also observed in our MD simulations. We have investigated the size distribution and chemical composition of the oxide fragments in the three systems. Here, a fragment is defined as consisting of covalently bonded atoms. At 200 ps, the percentages of the small sized fragments in all three systems are around or above 85% (88% for C3, 84% for C6, and 99% for C9), while the total number of fragments increases from around thousands to about 30, 90, and 200 thousands in the C3, C6, and C9, respectively. In all three systems, there is only one fragment having the number of atoms larger than 1000, which is the shell consisting of 2,978,188, 3,156,289, and 3,544,013 atoms for C3, C6, and C9, respectively. Table II lists the number of fragments for various chemical compositions in C3, C6, and C9 at 200 ps, where a transition from Al-rich to O-rich in the chemical composition of the major fragments is clearly seen when the initial temperature of the system is increased. In C3 and C6, majority of the fragments are formed inside the nanoparticle, but in C9 they are mostly outside. Oxidation rate of the outside fragments is much higher than that of the inside ones due to their easy access to oxygen.

We have also investigated the formation of hot spots and the effect of the initial core temperatures on it. Figure 4 shows the temperature distributions of all systems at 200 ps. Compared to C3, hot regions in C6 and C9 extend beyond the nanoparticle, and the temperature drop from the center to the surrounding is more continuous in C6 and C9. However, the hottest region in C6 is still near the nanoparticle, whereas it extends far beyond the nanoparticle in C9. The different sizes and magnitudes of the hot spots confirm that the mechanically enhanced reaction process in C9 forms a much greater hot spot than the other two systems in which the oxidation is only by diffusion.

In summary, we have found a fast reaction mechanism in which the opening of pores in the oxide shell at higher core temperatures lead to faster and more complete oxidation of nanoparticles, resulting in higher energy release rates. Catastrophic failure of the shell enhances the oxidation process by weakening or destroying the protective shell of the ANP, thereby providing pathways for ballistic transport of core Al. Faster oxidation due to higher core temperatures is evidenced by the production of more oxygen-rich molecular fragments at earlier times. The effect of the core temperature on the oxidation process and the energy release rate in our simulations is consistent with Dlott's experiments. Experiments by Zachariah's group have confirmed the formation of hollow ANP after the oxidation at elevated temperatures.[17]

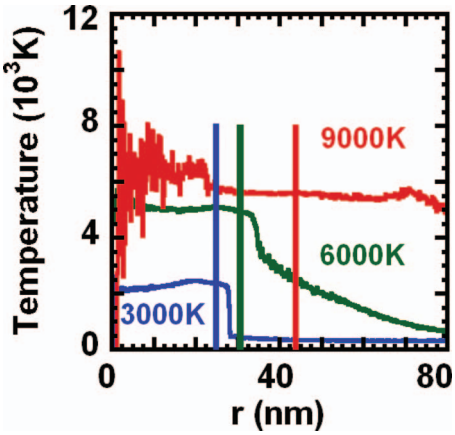

FIG. 4. (Color) Temperature profile of the C3, C6, and C9 systems at 200 ps. Temperature is averaged over a 2 Å thick shells. The higher initial core temperature results in the largest hotspot in C9. Three vertical bars, blue for C3, green for C6, and red for C9, have been added to indicate the outermost surface of the nanoparticle.

This work was supported by the Basic Research Program of Defense Threat Reduction Agency. Simulations were performed at the CACS and HPC center at USC. We thank Dr. Suhithi Peiris for stimulating discussions.

[1] B. W. Asay, S. E. Son, J. R. Busse, and D. M. Oschwald, Propellants, Explos., Pyrotech. **29**, 216 (2004).
[2] B. S. Bockmon, M. L. Pantoya, S. F. Son, B. W. Asay, and J. T. Mang, J. Appl. Phys. **98**, 064903 (2005).
[3] V. I. Levitas, B. W. Asay, S. F. Son, and M. Pantoya, J. Appl. Phys. **101**, 083524 (2007).
[4] S. F. Son, B. W. Asay, T. J. Foley, R. A. Yetter, M. H. Wu, and G. A. Risha, J. Propul. Power **23**, 715 (2007).
[5] C. Rossi and D. Esteve, Sens. Actuators, A **120**, 297 (2005).
[6] Y. Q. Yang, S. F. Wang, Z. Y. Sun, and D. D. Dlott, J. Appl. Phys. **95**, 3667 (2004).
[7] Y. Yang, S. Wang, Z. Sun, and D. D. Dlott, Appl. Phys. Lett. **85**, 1493 (2004).
[8] S. Wang, Y. Yang, H. Yu, and D. D. Dlott Propellants, Explos., Pyrotech. **30**, 148 (2005).
[9] A. Rai, D. Lee, K. Park, and M. R. Zachariah, J. Phys. Chem. B **108**, 14793 (2004).
[10] P. Vashishta, R. K. Kalia, A. Nakano, and J. P. Rino, J. Appl. Phys. **103**, 083504 (2008); **105**, 059901 (2009).
[11] A. F. Voter and S. P. Chen, Mater. Res. Soc. Symp. Proc. **896**, 0896-H03-05 (1987).
[12] Y. Q. Yang, Z. Y. Sun, S. F. Wang, and D. D. Dlott, J. Phys. Chem. B **107**, 4485 (2003).
[13] S. F. Wang, Y. Q. Yang, Z. Y. Sun, and D. D. Dlott, Chem. Phys. Lett. **368**, 189 (2003).
[14] N. N. Thadhani, J. Appl. Phys. **76**, 2129 (1994).
[15] T. J. Campbell, G. Aral, S. Ogata, R. K. Kalia, A. Nakano, and P. Vashishta, Phys. Rev. B **71**, 205413 (2005).
[16] T. N. Piehler, F. C. Delucia, C. A. Munson, B. E. Homan, A. W. Miziolek, and K. L. Mcnesby, Appl. Opt. **44**, 3654 (2005).
[17] A. Rai, L. Zhou, A. Prakash, A. Mccormick, and M. R. Zachariah, Mater. Res. Soc. Symp. Proc. **82**, 175 (2006).